AMERICAN SOCIETY FOR MICROBIOLOGY | Applied and Environmental Microbiology®

ENVIRONMENTAL MICROBIOLOGY

Ultrastructure of Organohalide-Respiring *Dehalococcoidia* Revealed by Cryo-Electron Tomography

Danielle L. Sexton,[a] Gao Chen,[b,c] Fadime Kara Murdoch,[b*] Ameena Hashimi,[a] Frank E. Löffler,[b,c,d,e,f] Elitza I. Tocheva[a]

[a]Department of Microbiology and Immunology, Life Sciences Institute, Health Sciences Mall, The University of British Columbia, Vancouver, British Columbia, Canada
[b]Center for Environmental Biotechnology, University of Tennessee, Knoxville, Tennessee, USA
[c]Department of Civil and Environmental Engineering, University of Tennessee, Knoxville, Tennessee, USA
[d]Department of Microbiology, University of Tennessee, Knoxville, Tennessee, USA
[e]Department of Biosystems Engineering & Soil Science, University of Tennessee, Knoxville, Tennessee, USA
[f]Biosciences Division, Oak Ridge National Laboratory, Oak Ridge, Tennessee, USA

Danielle L. Sexton and Gao Chen contributed equally to this work. Author order was determined based on increasing seniority.

ABSTRACT *Dehalococcoides mccartyi* (*Dhc*) and *Dehalogenimonas* spp. (*Dhgm*) are members of the class *Dehalococcoidia*, phylum Chloroflexi, characterized by streamlined genomes and a strict requirement for organohalogens as electron acceptors. Here, we used cryo-electron tomography to reveal morphological and ultrastructural features of *Dhc* strain BAV1 and "*Candidatus* Dehalogenimonas etheniformans" strain GP cells at unprecedented resolution. *Dhc* cells were irregularly shaped discs (890 ± 110 nm long, 630 ± 110 nm wide, and 130 ± 15 nm thick) with curved and straight sides that intersected at acute angles, whereas *Dhgm* cells appeared as slightly flattened cocci (760 ± 85 nm). The cell envelopes were composed of a cytoplasmic membrane (CM), a paracrystalline surface layer (S-layer) with hexagonal symmetry and ~22-nm spacing between repeating units, and a layer of unknown composition separating the CM and the S-layer. Cell surface appendages were only detected in *Dhc* cells, whereas both cell types had bundled cytoskeletal filaments. Repetitive globular structures, ~5 nm in diameter and ~9 nm apart, were observed associated with the outer leaflet of the CM. We hypothesized that those represent organohalide respiration (OHR) complexes and estimated ~30,000 copies per cell. In *Dhgm* cultures, extracellular lipid vesicles (20 to 110 nm in diameter) decorated with putative OHR complexes but lacking an S-layer were observed. The new findings expand our understanding of the unique cellular ultrastructure and biology of organohalide-respiring *Dehalococcoidia*.

IMPORTANCE *Dehalococcoidia* respire organohalogen compounds and play relevant roles in bioremediation of groundwater, sediments, and soils impacted with toxic chlorinated pollutants. Using advanced imaging tools, we have obtained three-dimensional images at macromolecular resolution of whole *Dehalococcoidia* cells, revealing their unique structural components. Our data detail the overall cellular shape, cell envelope architecture, cytoskeletal filaments, the likely localization of enzymatic complexes involved in reductive dehalogenation, and the structure of extracellular vesicles. The new findings expand our understanding of the cell structure-function relationship in *Dehalococcoidia* with implications for *Dehalococcoidia* biology and bioremediation.

KEYWORDS Dehalococcoidia, cryo-electron tomography, organohalide respiration (OHR) complexes, ultrastructure

Dehalococcoidia are broadly distributed in environmental systems where they take advantage of naturally occurring organohalogens (1). Significant interest in this class within the Chloroflexi has arisen for the application of organohalide-respiring

Editor Jeremy D. Semrau, University of Michigan-Ann Arbor

Address correspondence to Frank E. Löffler, frank.loeffler@utk.edu, or Elitza I. Tocheva, elitza.tocheva@ubc.ca.

*Present address: Fadime Kara Murdoch, Battelle Memorial Institute, Columbus, Ohio, USA.

The authors declare no conflict of interest.

Received 25 September 2021
Accepted 30 October 2021
Accepted manuscript posted online 17 November 2021
Published 25 January 2022

Dehalococcoidia in bioremediation of groundwater aquifers and sediments contaminated with toxic chlorinated compounds such as chlorinated solvents (2, 3) and polychlorinated biphenyls (PCBs) (4–7). To date, all *Dehalococcoides mccartyi* (*Dhc*) and *Dehalogenimonas* spp. (*Dhgm*) isolates have been enriched and isolated with chlorinated electron acceptors that are categorized as environmental pollutants. The cultivated members of the class *Dehalococcoidia* grow fastidiously in axenic culture, all share the obligate organohalide-respiring phenotype and strictly depend on certain chlorinated organic compounds as electron acceptors (3, 8). *Dhc* requires hydrogen as electron donor for reductive dechlorination, whereas the characterized *Dhgm* species can also couple formate oxidation to reductive dechlorination (9, 10).

The first *Dehalococcoidia* isolate, *Dhc* strain 195, was described in 1997 and transmission electron microscopy (TEM) images revealed small, irregular coccoid cells with an unusual cell wall ultrastructure resembling the surface layer (S-layer) of Archaea (11). Phase-contrast light microscopy analysis of *Dhc* cells suggested a disc-shaped morphology with cell thickness of less than 0.2 μm (2, 3). Subsequent TEM and scanning electron microscopy (SEM) studies revealed round to irregular, disc-shaped *Dhc* cells 0.3 to 1 μm wide and 0.1 to 0.2 μm thick with characteristic biconcave indentations on opposite flat sides of the cell (2, 3). *Dhgm* isolates were described as cocci 0.3 to 0.6 μm in diameter (12). Sample preparation for both TEM and SEM relies on dehydration and plastic embedding, thus potentially introducing artifacts that can lead to unusual cell shapes with no biological relevance, rendering the interpretation of imaging results ambiguous. Successive efforts to reveal the cellular ultrastructure of organohalide-respiring *Dehalococcoidia* have been at a standstill.

A shared feature among the available *Dhc* and *Dhgm* genomes is the presence of multiple, nonidentical reductive dehalogenase (*rdhA*) genes encoding a catalytic subunit. A few RdhA have been studied in detail and common features have emerged: RdhA proteins represent a novel class of cobamide-containing oxidoreductases that are composed of approximately 500 amino acids, are sensitive to oxygen, harbor two Fe-S clusters, contain a cobamide prosthetic group, and have a twin-arginine translocation (TAT) signal peptide at the N-terminus (13–16). Biochemical evidence suggests that *in vivo*, RdhA is tethered to the outside of the cytoplasmic membrane (CM) via a small, 90 to 100 amino acid-long integral membrane anchor protein RdhB (17, 18). The RdhA enzymes have been shown to form a higher molecular weight complex with hydrogen-uptake (Hup) hydrogenases and two organohalide respiration-involved molybdoenzyme (Ome) subunits collectively termed the organohalide respiration (OHR) complex (19). Based on available genome information, OHR complexes of *Dhc* strains and *Dhgm* species have a predicted mass of around 350 kDa, and experimentally measured molecular masses ranging between 250 and 270 kDa (17, 18, 20). Therefore, these complexes are large enough to be visualized directly by cryo-electron tomography (cryo-ET). Cryo-ET is an approach that allows for the direct imaging of whole bacterial cells in their native state and in three dimensions. By plunge-freezing the sample into liquid ethane at −196°C, cells are preserved on electron microscopy (EM) grids without additional manipulation. In contrast to TEM and SEM, cryogenically preserved biological samples, including bacterial cells, maintain their cellular ultrastructure and macromolecules can be resolved at 2 to 4 nm resolution (21).

To advance our understanding of the morphological and ultrastructural features of *Dhc* and *Dhgm* cells, we performed cryo-ET on axenic cultures of *Dhc* strain BAV1 and "*Candidatus* Dehalogenimonas etheniformans" strain GP. Our data reveal unprecedented cellular details, including overall cell morphology, S-layer structure, cell envelope architecture, cytoskeletal filaments, extracellular vesicles, and the likely localization of the membrane-associated OHR complex.

RESULTS

Phylogeny. The class *Dehalococcoidia* of the phylum Chloroflexi currently comprises two genera with validly published names, *Dehalococcoides* and *Dehalogenimonas*, and

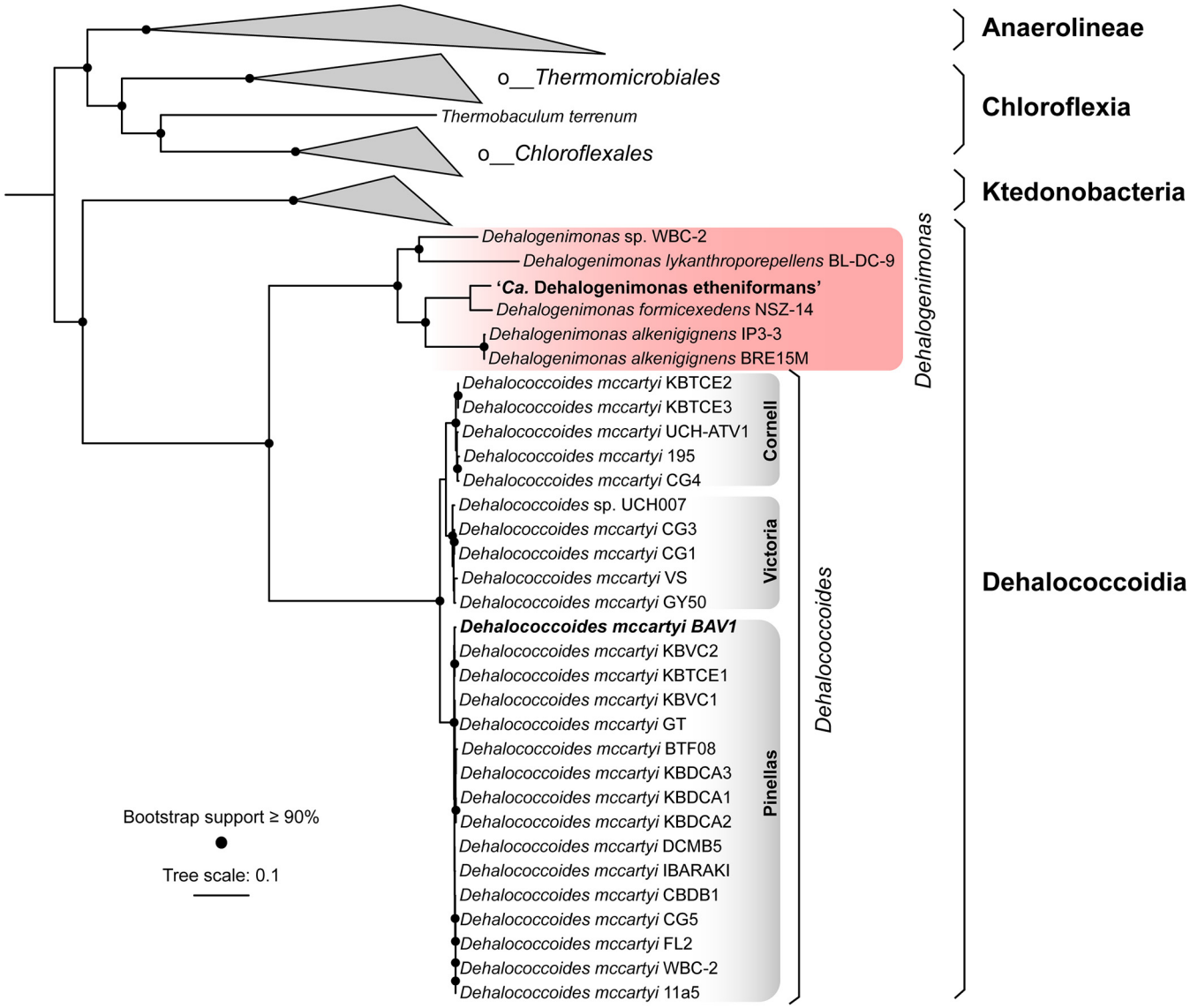

FIG 1 Phylogeny of *Dehalococcoidia*. The tree was constructed using an alignment of 120 conserved single-copy genes obtained using the GTDB-Tk and the maximum-likelihood algorithm. Bootstrap values ≥ 90% are shown. Scale bar represents 0.1 substitutions per site. Classes within the Chloroflexi phylum are labeled on the right in bold, and clades *Thermomicrobiales*, *Chloroflexales*, *Dehalogenimonas*, and *Dehalococcoides* are shown in italics. Labels correspond to the taxonomy proposed by the GTDB.

accommodates the "*Candidatus* Dehalobium chlorocoercia" strain DF-1. All available *Dehalococcoides* isolates belong to a single species, *Dehalococcoides mccartyi* (3). The taxonomic grouping in the *Dhgm* genus follows a different approach, and four species, each represented by a single-type strain, have been validly named (22). Fig. 1 illustrates a phylogeny of the class *Dehalococcoidia* calculated based on the maximum likelihood algorithm and the relationships between *Dhc* and *Dhgm*. The topology of the tree based on the concatenated alignment of 120 conserved genes (Fig. 1) was consistent with the 16S rRNA gene-based phylogenetic tree (Fig. S1).

Cellular ultrastructure. Consistent with the phylogenetic separation of the genera *Dehalococcoides* and *Dehalogenimonas*, cryo-ET imaging revealed distinct morphological features. *Dhc* strain BAV1 cells ($n = 10$) were thin, irregularly shaped discs approximately 890 ± 110 nm long, 630 ± 110 nm wide, and 130 ± 15 nm thick (Fig. 2, Table 1). *Dhc* cells frequently had between 6 to 10 straight sides that intersected at acute angles, though it was not uncommon to see curved sides as well (Fig. 2A and G). Cryo-ET did not reveal indentations in these cells as previously observed in SEM studies

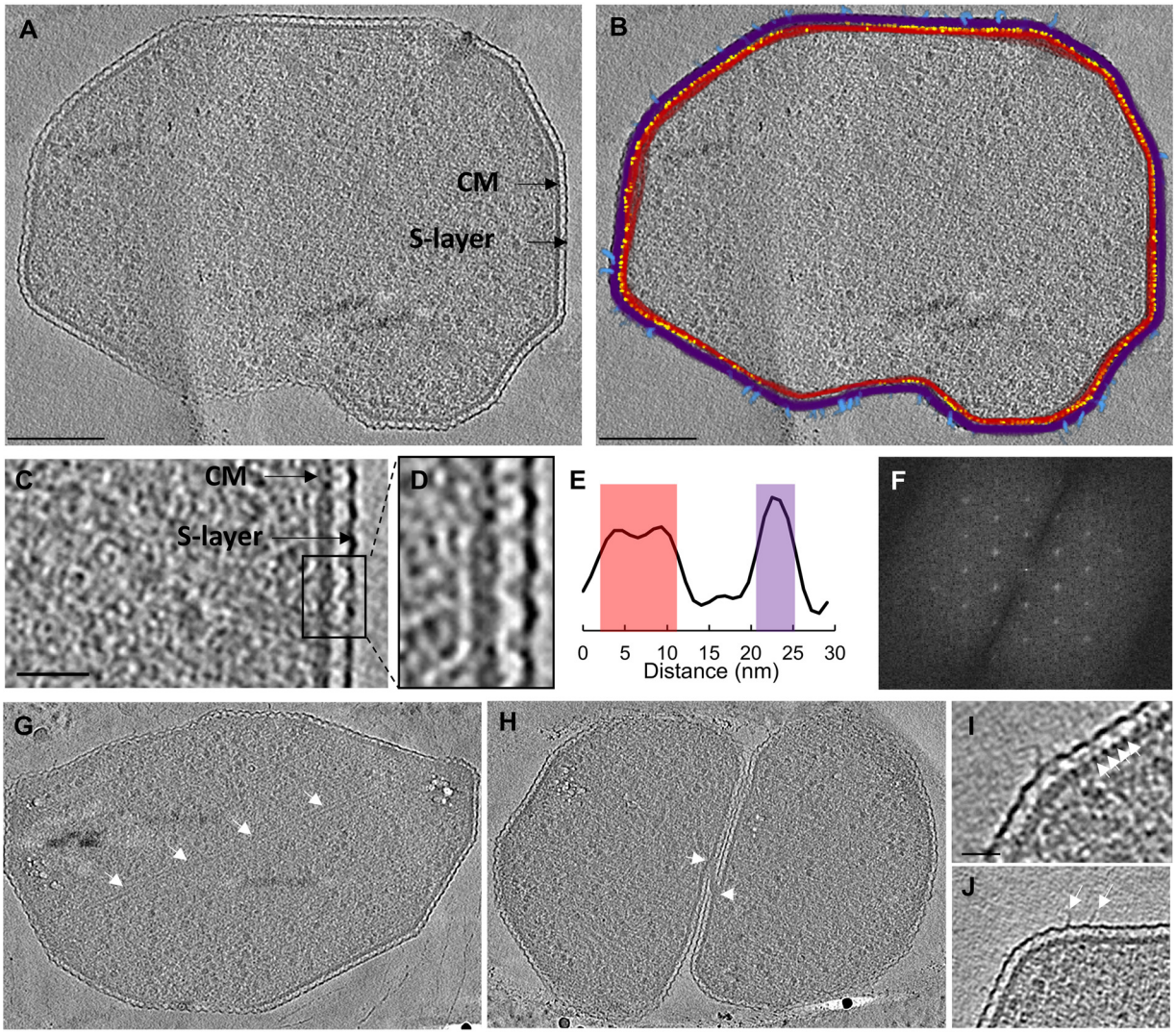

FIG 2 Ultrastructure of *Dhc* strain BAV1 cells revealed by cryo-ET. (A) A 20-nm thick slice through a *Dhc* tomogram highlighting the irregular cell shape. (B) Segmentation showing the CM (red), putative OHR complexes (yellow), the S-layer (purple), and surface appendages (light blue). Scale bar, 200 nm. (C) and (D) Enlarged views of the cell envelope show the bilayer of the CM and the S-layer. Scale bar, 50 nm. (E) Density profile of the cell envelope with CM in red and S-layer in purple. (F) Diffraction pattern of the S-layer shows hexagonal packing of the surface proteins with 22-nm spacing. Major features in G–J are highlighted with white arrows. (G) Cytoskeletal filaments spanning the long axis of the cell. (H) A tubular structure connecting two adjacent cells. (I) A section of the CM loaded with putative OHR complexes spaced ~9 nm apart. Scale bar, 20 nm. (J) Surface appendages associated with the S-layer.

(2, 3) suggesting that those indentations resulted from sample preparation and are an artifact. "*Ca*. Dehalogenimonas etheniformans" strain GP cells ($n = 10$) were slightly flattened cocci with an average diameter of 760 nm (Fig. 3, Table 1).

Despite differences in cell morphology, both *Dhc* and *Dhgm* had similar cell envelope architectures. The cell envelope consisted of the CM and a prominent S-layer (Fig. 2C to E, 3C to E). The paracrystalline S-layer in both strains showed hexagonal symme-

TABLE 1 Dimensions of *Dhc* strain BAV1 and *Dhgm* strain GP cells determined by cryo-ET

Cell dimensions (nm)	*Dhc* strain BAV1[a]	*Dhgm* strain GP[a]
Length	890 ± 110	760 ± 85
Width	630 ± 110	765 ± 85
Thickness[b]	130 ± 15	325 ± 90

[a]$n = 10$.
[b]Flattening of cells can result from the vitrification process.

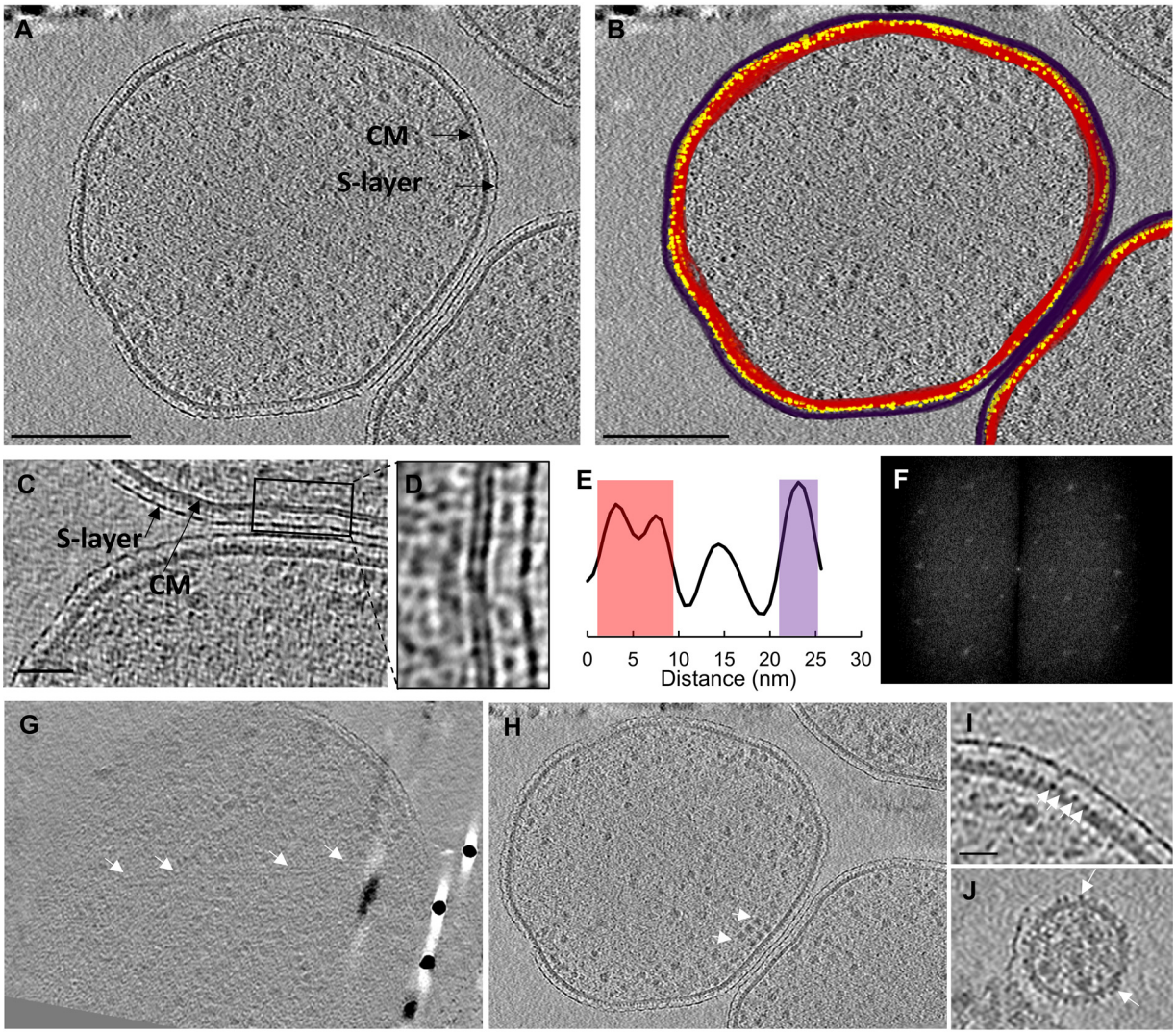

FIG 3 Ultrastructure of *Dhgm* strain GP cells revealed by cryo-ET. (A) A 20-nm thick slice through a *Dhgm* tomogram showing spherical cell morphology. (B) Segmentation highlighting the CM (red), putative OHR complexes (yellow), and the S-layer (purple). Scale bar, 200 nm. (C) and (D) Enlarged views of the cell envelope showing the bilayer of the CM and the S-layer. Scale bar, 50 nm. (E) Density profile of the cell envelope with the density of the CM in red and the S-layer in purple. (F) Diffraction pattern of the S-layer shows hexagonal packing of the surface proteins with 21-nm spacing. Major features in G–J are highlighted with white arrows. (G) Cytoskeletal filaments spanning the cell. (H) Polysomes associated with the CM. (I) A section of the CM loaded with putative OHR complexes spaced ~9 nm apart. Scale bar, 20 nm. (J) Extracellular vesicles enclosed by a lipid bilayer containing putative OHR complexes.

try with ~22-nm spacing between repeating units (Fig. 2F, 3F). When density profiles were calculated for both cell types (Fig. 2E, 3E), a layer of unknown composition could be resolved between the CM and the S-layer. The unknown layer appeared more prominent in the *Dhgm* cells (Fig. 3E) than in the *Dhc* cells (Fig. 2E).

The cryotomograms revealed filamentous structures, tubular connections, surface appendages, and polysomes (i.e., clusters of ribosomes). The filaments observed in *Dhc* cells were organized in a bundle, ~800 nm long and ~50 nm wide, and spanned the long axis of the cell without apparent contact with the CM (Fig. 2G). Similar, yet less pronounced bundles were observed in *Dhgm* cells (Fig. 3G). Occasionally, *Dhc* cells were observed interconnected to each other via thin tubular structures (Fig. 2H). Outward-directed appendages with a diameter of ~3 nm that varied in length between 10 and 30 nm (average length ~13 nm) were distributed along the surface of *Dhc* cells and appeared connected to the S-layer (Fig. 2B and J). The appendages surrounding *Dhc* cells were most frequently located at or near points where the sides of

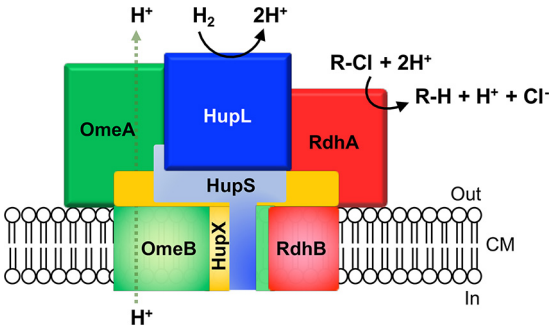

FIG 4 Model of the OHR complex based on published data (17–20). The OHR complex is predicted to be a fully functional, stand-alone respiratory chain in *Dhc* and *Dhgm*. The OHR complex includes the following components: a hydrogen uptake hydrogenase Hup (with its large and small catalytic subunits HupL and HupS, respectively), a protein with four predicted Fe-S clusters (HupX), the organohalide respiration-involved molybdoenzyme (OmeA) with its putative integral membrane anchoring protein OmeB, and an RdhA reductive dehalogenase with its integral membrane protein anchor RdhB.

the cells formed acute angles (Fig. 2B and J). Similar appendages were not detected on the surface of *Dhgm* cells. Polysomes observed in the cytoplasm of *Dhgm* cells were associated with the CM (Fig. 3H).

OHR complex. The genomes of *Dhc* strain BAV 1 and *Dhgm* strain GP are available (10, 23) and both comprise the full set of genes encoding the OHR complex. The components of the OHR complex are illustrated in Fig. 4 and their respective sizes listed in Table 2. BvcA (DehaBAV1_0847) is the VC RdhA of *Dhc* strain BAV1 (24, 25), and CerA (HX448_10020) functions as the VC RdhA in *Dhgm* strain GP (26). Of note, at least some of the complex components (e.g., OmeB, RdhB) are partly embedded or integral membrane proteins and thus not part of the periplasmic portion of the OHR complex.

The CMs of both isolates were rich in repetitive globular structures associated with the periplasmic side of the membrane. The observed structures were membrane-associated because, when bound, the two leaflets of the CM could not be resolved. This observation suggested that the integral membrane proteins anchored the complex to the CM. Our cryotomograms revealed that the globular structures were ~5 nm in diameter and ~9 nm apart (Fig. 2I, 3I, also see supplemental material). Based on their subcellular location, association with the CM and abundance, we hypothesized that these globular structures represent OHR complexes. We estimated that the complexes occupy ~2/3 of the membrane surface area in both *Dhc* strain BAV1 and *Dhgm* strain GP cells. Assuming the ~9-nm spacing between complexes was maintained throughout the cell surface, we calculated ~30,000 OHR complexes per cell for both organisms. The bilayer of the CM could be resolved in regions where the putative OHR com-

TABLE 2 Homologous OHR complex proteins encoded by the genomes of *Dhc* strain BAV1 and *Dhgm* strain GP

	Dhc strain BAV1[a]		*Dhgm* strain GP'[b]	
OHR complex protein	Gene locus tag	Molecular mass (kDa)	Gene locus tag	Molecular mass (kDa)
OmeA	DehaBAV1_0165	105.7	HX448_03695	117.8
OmeB	DehaBAV1_0166	44.8	HX448_03705	42.7
HupL	DehaBAV1_0258	58.0	HX448_00350	56.8
HupS	DehaBAV1_0257	37.1	HX448_00345	36.9
HupX	DehaBAV1_0256	30.4	HX448_00340	29.5
RdhA	DehaBAV1_0847 (BvcA)	57.4	HX448_10020 (CerA)	62.0
RdhB	Not identified (BvcB)[c]	10.1[c]	HX448_10015 (CerB)	11.0

[a]Genome accession number: CP000688.1.
[b]Genome accession number: CP058566.2.
[c]BvcB in *Dhc* strain BAV1 has not been identified and its size was estimated based on the average size of the nine RdhB encoded on the strain BAV1 genome.

plexes were absent (Fig. 2E, 3E). A notable observation in cultures of *Dhgm* strain GP was the presence of numerous extracellular lipid vesicles ranging in size from 20 nm to 110 nm (Fig. 3J, Fig. S2). The vesicles were formed by the CM, had membrane-associated complexes and lacked an S-layer (Fig. 3J). Additional images of these extracellular lipid vesicles observed in *Dhgm* strain GP along with size measurements are shown in Fig. S2.

DISCUSSION

Cell morphology and cell envelope characteristics. Cryotomograms of *Dhc* and *Dhgm* cells revealed that both bacteria have a cell envelope with a clearly visible CM and an S-layer, consistent with prior TEM and SEM imaging results (2, 3, 11, 27). Cryo-ET detected an additional layer of unknown composition located between the CM and S-layer in both organisms, which appeared more prominent in *Dhgm* cells (Fig. 3E). Because both *Dhc* and *Dhgm* lack the capability for peptidoglycan (PG) biosynthesis (3, 11, 12, 28), it is possible that this layer is part of the S-layer proteins involved in anchoring to the CM, or has a novel composition altogether. Typically, PG dictates cell shape in bacteria. In its absence, however, cell morphology can be controlled by cytoskeletal elements as was shown for *Mycoplasma* (29, 30). While bundled cytoskeletal filaments were observed in both *Dhc* strain BAV1 and *Dhgm* strain GP, these filaments did not appear to directly interact with the CM (Fig. 2G, 3G). The striking differences in cell morphology between the irregular flat discs of *Dhc* and the regular cocci of *Dhgm* suggest that there may be unique structural differences governing cell morphology in these bacteria.

Within the domain Archaea, flat irregular cell morphologies have been attributed to the arrangement of S-layer proteins and capsular polysaccharides (31–33). In *Dhc* strain 195, proteomic studies identified the S-layer protein DET1407 in membrane-enriched fractions (34). DET1407 (GenBank accession # AAW39334.1) is a 105.5 kDa protein annotated as a BNR/Asp-box repeat domain protein. Comparative sequence analysis showed low similarity of DET1407 with some structural proteins such as bacteriophage capsid proteins, and it was suggested that this protein resembles membrane-bound archaeal type S-layer proteins (34). Homologs of DET1407 were found in the genomes of *Dhc* strain BAV1 (WP_012034154.1; locus tag: DehaBAV1_1214) (23) and *Dhgm* strain GP (WP_102331005.1; locus tag: HX448_00895) (10) with amino acid sequence identities of 72% and 33%, respectively. Analysis of the putative S-layer proteins in *Dhc* and *Dhgm* with the TMHMM Server v.2.0 (35) identified transmembrane domains at both ends of the proteins that could serve as membrane anchors. Structural differences in S-layer proteins between *Dhc* and *Dhgm* strains could account for the observed variations in cell shape.

The surface appendages on *Dhc* but not on *Dhgm* cells could also be responsible for the differences in cell morphology. In *Dhc* cells, the surface appendages were most often detected in the S-layer at points with acute angles. It is possible that the integration of the appendages into the S-layer alters the arrangement of S-layer proteins, introducing sharp angles into the S-layer. Previous negative-stained TEM images of *Dhc* strain DCMB5 revealed filamentous structures resembling type IV pili (36). The surface appendages observed in our cryotomograms of *Dhc* strain BAV1 appear structurally distinct from the previously reported structures in *Dhc* strain DCMB5. The appendages are thinner, more abundant on the cell surface, and much shorter than typical type IV pili. Thus, we speculate that the appendages are distinct structures, and similarly to the type IV pili, could be involved in surface attachment.

OHR complexes in *Dehalococcoidia*. Clearly resolved globular periplasmic complexes were associated with the CM in both *Dhc* and *Dhgm* cells (Fig. 2I, 3I). Previous biochemical studies using cell membrane fractions of *Dehalococcoidia* cultures detected OHR complex proteins and did not detect the expression of other macromolecular assemblies such as complex I (NADH quinone oxidoreductase) (17, 20, 37). Therefore, the OHR complex is likely the only membrane-associated periplasmic

protein complex present in these bacteria during growth via organohalide respiration (17, 19, 20).

Our cryotomograms reveal 5-nm globular structures associated with the outer leaflet of the CM. These 5-nm globular structures were abundant and evenly spaced (Fig. 2I, 3I); however, their distribution around the cells was not uniform (Fig. 2B, 3B). Based on the cryo-ET imaging results, we estimate that a single *Dhc* or *Dhgm* cell harbors ~30,000 putative OHR complexes when grown with VC as electron acceptor. Previous characterization of OHR complexes in *Dhc* and *Dhgm* found a single RdhA molecule per complex (17, 20). TceA is a *Dhc* RdhA implicated in trichloroethene to ethene reductive dechlorination (38), and prior proteomic work estimated TceA abundances ranging between 1,800 and 26,000 molecules per *Dhc* cell in different *Dhc*-containing mixed cultures (39, 40). Our estimates based on cryo-ET imaging support the upper range for RdhA proteins in OHR complexes per cell. Significantly lower RdhA abundances not exceeding 115 protein molecules per cell were reported in axenic *Dhc* strain CBDB1 cultures grown with hexachlorobenzene as electron acceptor (41). Future work will determine if the numbers of OHR complexes per cell vary in response to environmental conditions, or if viable *Dehalococcoidia* cells maintain a constant number of (active) OHR complexes. The expression of multiple RdhA enzymes has been demonstrated in axenic *Dhc* cultures (38); however, it is unclear if a single cell carries OHR complexes with different RdhA, or if distinct cell populations exist. The OHR complexes in *Dhc* and *Dhgm* have been described as modular (17, 19, 20); however, it remains to be determined whether the RdhA component of an already-assembled OHR complex can be exchanged. The periplasmic location of the complex makes exchange unlikely, suggesting that new complexes with a different RdhA component would require the synthesis of new cells.

Extracellular lipid vesicles were observed only in cryotomograms of *Dhgm* cells (Fig. 3J, Fig. S2), although similar structures were previously detected in axenic *Dhc* cultures by SEM (3, 42), suggesting these structures occur in both genera. The biological significance of these vesicles is uncertain, but it has been speculated that they play a role in horizontal gene transfer and are formed in response to unfavorable growth conditions (43, 44). The cryo-ET images further show that the vesicles contain OHR complexes, although it remains to be determined whether these structures contribute to reductive dechlorination activity. Field monitoring using qPCR to enumerate *Dhc* biomarker genes revealed that the abundance of a *Dhc rdhA* gene (e.g., *tceA*) can exceed the total *Dhc* cell abundance by up to four orders of magnitude; however, no additional dechlorination activity was measured (44). These field observations could be explained by the presence of extracellular lipid vesicles that contain DNA and are enriched in *rdhA* genes relative to *Dhc* 16S rRNA genes without contributing to reductive dechlorination activity (i.e., the OHR complexes in vesicles are not active).

Taken together, the application of cryo-ET revealed unprecedented insights into ultrastructural features of *Dhc* and *Dhgm* cells, foremost the likely sub-cellular localization and abundance of the membrane-associated OHR complex in the periplasmic space. The integrated application of advanced imaging techniques, such as cryo-ET, with genetic, biochemical, and physiological experimentation promises to reveal new insights into the biology of these fascinating bacteria, whose energy metabolism strictly depends on halogenated electron acceptors.

MATERIALS AND METHODS

Phylogenetic analysis. A representative phylogeny using the maximum-likelihood algorithm was determined by extracting an alignment of 120 conserved bacterial single-copy marker genes (45) from representative Chloroflexi members using the Genome Taxonomy Database GTDB-Tk v1.1.0 software (46). The tree was constructed using IQ-TREE (v. 2.0.3) with 1,000 ultrafast bootstraps and the substitution model LG+F+R5, as determined by ModelFinder (47, 48). Genes of representative Firmicutes genomes served as outgroups. To construct a 16S rRNA gene phylogenetic tree, Chloroflexi sequences were obtained from the SILVA database (49), and a single 16S rRNA gene sequence per genome was selected for subsequent analysis. Sequences were aligned using MUSCLE (50), and trimmed to 1,429 aligned positions using ClipKIT with the medium-gappy parameter (51). The 16S rRNA gene tree was

constructed using IQ-TREE with the HKY85 model and 1,000 ultrafast bootstraps. The trees were visualized using iTOL (v4) (52). "*Candidatus* Dehalobium chlorocoercia" strain DF-1 (53, 54), possibly a member of the *Dehalococcoidia*, was excluded from the phylogenetic analysis as the genome was unavailable.

Growth of *Dhc* strain BAV1 and *Ca.* Dehalogenimonas etheniformans strain GP. Routine cultivation of *Dhc* and *Dhgm* isolates was performed in 160-ml glass serum bottles containing 100 ml of bicarbonate-buffered (30 mM, pH 7.2) mineral salt medium (55, 56). The vessels were sealed with black butyl rubber stoppers (Bellco Glass Inc., Vineland, NJ) under a headspace of N_2/CO_2 (80/20, vol/vol) and vinyl chloride (VC, ~40 μmol per bottle with two additional feedings) was provided as electron acceptor. The *Dhc* and *Dhgm* cultures received H_2 (~410 μmol per bottle) or formate (5 mM), respectively, as electron donor. Acetate (5 mM) was provided as the carbon source. Growth was monitored by measuring the consumption of VC and the formation of ethene via headspace injection using an Agilent 7890A gas chromatograph (Santa Clara, CA) equipped with a DB-624 column (60 m length, 0.32 mm inner diameter, 1.8 μm film thickness) and a flame ionization detector (57).

Cryo-ET data collection and processing. Bacterial cultures were mixed with 20-nm colloidal gold particles and loaded onto glow-discharged R2/2 Quantifoil carbon grids (EMS, Hatfield, PA). Samples were then plunge-frozen into a liquid ethane-propane mixture cooled at liquid nitrogen temperatures with a Mark IV Vitrobot maintained at room temperature and 70% humidity. Tilt series were collected at 4 μm defocus, 90 e-/Å^2 total dose, $\pm$ 60° bidirectional tilt, and 1° increments using SerialEM software (58) on a Titan Krios 300 kV transmission electron microscope (Thermo Fisher Scientific) equipped with a Falcon III direct electron detector camera. Three-dimensional reconstructions were calculated using the IMOD package and the back-weighted projection method (59). Density profiles were calculated using ImageJ (60) and segmentations were generated using Dragonfly 2020.2. Calculations of the number of putative OHR complexes was based on our cryotomograms. To calculate cell surface area, we used ellipsoid and sphere approximations for *Dhc* and *Dhgm* cells, respectively. The supplemental material provides a detailed description of the calculations.

SUPPLEMENTAL MATERIAL

Supplemental material is available online only.

SUPPLEMENTAL FILE 1, PDF file, 1.6 MB.

ACKNOWLEDGMENTS

F.E.L. acknowledges support from The University Consortium for Field-Focused Groundwater Research. Work in the EIT Lab was supported by a Natural Sciences and Engineering Research Council of Canada Discovery Grant (RGPIN 04345). D.L.S. was supported by a Natural Sciences and Engineering Research Council of Canada Postdoctoral Fellowship (546024).

We thank Florian Rossman and the High Resolution Macromolecular Cryo-Electron Microscopy facility at the University of British Columbia for assistance with microscope operation and tilt series acquisition.

REFERENCES

1. Yang Y, Sanford R, Yan J, Chen G, Cápiro NL, Li X, Löffler FE. 2020. Roles of organohalide-respiring *Dehalococcoidia* in carbon cycling. mSystems 5:e00757-19. https://doi.org/10.1128/mSystems.00757-19.
2. He J, Ritalahti KM, Yang K-L, Koenigsberg SS, Löffler FE. 2003. Detoxification of vinyl chloride to ethene coupled to growth of an anaerobic bacterium. Nature 424:62–65. https://doi.org/10.1038/nature01717.
3. Löffler FE, Yan J, Ritalahti KM, Adrian L, Edwards EA, Konstantinidis KT, Müller JA, Fullerton H, Zinder SH, Spormann AM. 2013. *Dehalococcoides mccartyi* gen. nov., sp. nov., obligately organohalide-respiring anaerobic bacteria relevant to halogen cycling and bioremediation, belong to a novel bacterial class, *Dehalococcoidia* classis nov., order *Dehalococcoidales* ord. nov. and family *Dehalococcoidaceae* fam. nov., within the phylum *Chloroflexi*. Int J Syst Evol 63:625–635. https://doi.org/10.1099/ijs.0.034926-0.
4. Bedard DL, Ritalahti KM, Löffler FE. 2007. The *Dehalococcoides* population in sediment-free mixed cultures metabolically dechlorinates the commercial polychlorinated biphenyl mixture Aroclor 1260. Appl Environ Microbiol 73:2513–2521. https://doi.org/10.1128/AEM.02909-06.
5. Adrian L, Dudková V, Demnerová K, Bedard DL. 2009. *Dehalococcoides* sp. strain CBDB1 extensively dechlorinates the commercial polychlorinated biphenyl mixture Aroclor 1260. Appl Environ Microbiol 75:4516–4524. https://doi.org/10.1128/AEM.00102-09.
6. Wang S, Chng KR, Wilm A, Zhao S, Yang K-L, Nagarajan N, He J. 2014. Genomic characterization of three unique *Dehalococcoides* that respire on persistent polychlorinated biphenyls. Proc Natl Acad Sci U S A 111:12103–12108. https://doi.org/10.1073/pnas.1404845111.
7. Payne RB, Ghosh U, May HD, Marshall CW, Sowers KR. 2019. A pilot-scale field study: in situ treatment of PCB-impacted sediments with bioamended activated carbon. Environ Sci Technol 53:2626–2634. https://doi.org/10.1021/acs.est.8b05019.
8. Yan J, Rash BA, Rainey FA, Moe WM. 2009. Isolation of novel bacteria within the *Chloroflexi* capable of reductive dechlorination of 1,2,3-trichloropropane. Environ Microbiol 11:833–843. https://doi.org/10.1111/j.1462-2920.2008.01804.x.
9. Key TA, Bowman KS, Lee I, Chun J, Albuquerque L, da Costa MS, Rainey FA, Moe WM. 2017. *Dehalogenimonas formicexedens* sp. nov., a chlorinated alkane-respiring bacterium isolated from contaminated groundwater. Int J Syst Evol 67:1366–1373. https://doi.org/10.1099/ijsem.0.001819.
10. Yang Y, Yan J, Li X, Lv Y, Cui Y, Kara Murdoch F, Chen G, Löffler FE. 2020. Genome sequence of "*Candidatus* Dehalogenimonas etheniformans" strain GP, a vinyl chloride-respiring anaerobe. Microbiol Resour Announc 9:e01212-20. https://doi.org/10.1128/MRA.01212-20.
11. Maymó-Gatell X, Chien Y-T, Gossett JM, Zinder SH. 1997. Isolation of a bacterium that reductively dechlorinates tetrachloroethene to ethene. Science 276:1568–1571. https://doi.org/10.1126/science.276.5318.1568.
12. Moe WM, Yan J, Nobre MF, da Costa MS, Rainey FA. 2009. *Dehalogenimonas lykanthroporepellens* gen. nov., sp. nov., a reductively dehalogenating bacterium isolated from chlorinated solvent-contaminated groundwater. Int J Syst Evol Microbiol 59:2692–2697. https://doi.org/10.1099/ijs.0.011502-0.
13. Hug LA, Maphosa F, Leys D, Löffler FE, Smidt H, Edwards EA, Adrian L. 2013. Overview of organohalide-respiring bacteria and a proposal for a

classification system for reductive dehalogenases. Philos Trans R Soc Lond B Biol Sci 368:20120322. https://doi.org/10.1098/rstb.2012.0322.
14. Hug LA. 2016. Diversity, evolution, and environmental distribution of reductive dehalogenase genes, p 377–393. *In* Adrian L, Löffler FE (ed), Organohalide-respiring bacteria. Springer Berlin Heidelberg, Berlin, Germany.
15. Fincker M, Spormann AM. 2017. Biochemistry of catabolic reductive dehalogenation. Annu Rev Biochem 86:357–386. https://doi.org/10.1146/annurev-biochem-061516-044829.
16. Yan J, Bi M, Bourdon AK, Farmer AT, Wang P-H, Molenda O, Quaile AT, Jiang N, Yang Y, Yin Y, Şimşir B, Campagna SR, Edwards EA, Löffler FE. 2018. Purinyl-cobamide is a native prosthetic group of reductive dehalogenases. Nat Chem Biol 14:8–14. https://doi.org/10.1038/nchembio.2512.
17. Kublik A, Deobald D, Hartwig S, Schiffmann CL, Andrades A, von Bergen M, Sawers RG, Adrian L. 2016. Identification of a multi-protein reductive dehalogenase complex in *Dehalococcoides mccartyi* strain CBDB1 suggests a protein-dependent respiratory electron transport chain obviating quinone involvement. Environ Microbiol 18:3044–3056. https://doi.org/10.1111/1462-2920.13200.
18. Schubert T, Adrian L, Sawers RG, Diekert G. 2018. Organohalide respiratory chains: composition, topology and key enzymes. FEMS Microbiol Ecol 94:fiy035.
19. Seidel K, Kühnert J, Adrian L. 2018. The complexome of *Dehalococcoides mccartyi* reveals its organohalide respiration-complex is modular. Front Microbiol 9:1130. https://doi.org/10.3389/fmicb.2018.01130.
20. Trueba-Santiso A, Wasmund K, Soder-Walz JM, Marco-Urrea E, Adrian L. 2021. Genome sequence, proteome profile, and identification of a multiprotein reductive dehalogenase complex in *Dehalogenimonas alkenigignens* strain BRE15M. J Proteome Res 20:613–623. https://doi.org/10.1021/acs.jproteome.0c00569.
21. Tocheva EI, Li Z, Jensen GJ. 2010. Electron cryotomography. Cold Spring Harb Perspect Biol 2:a003442. https://doi.org/10.1101/cshperspect.a003442.
22. Moe WM, Rainey FA, Yan J. 2016. The genus *Dehalogenimonas*, p 137–151. *In* Adrian L, Löffler FE (ed), Organohalide-respiring bacteria. Springer Berlin Heidelberg, Berlin, Heidelberg.
23. McMurdie PJ, Behrens SF, Müller JA, Göke J, Ritalahti KM, Wagner R, Goltsman E, Lapidus A, Holmes S, Löffler FE, Spormann AM. 2009. Localized plasticity in the streamlined genomes of vinyl chloride respiring *Dehalococcoides*. PLoS Genet 5:e1000714. https://doi.org/10.1371/journal.pgen.1000714.
24. Krajmalnik-Brown R, Hölscher T, Thomson IN, Saunders FM, Ritalahti KM, Löffler FE. 2004. Genetic identification of a putative vinyl chloride reductase in *Dehalococcoides* sp. strain BAV1. Appl Environ Microbiol 70:6347–6351. https://doi.org/10.1128/AEM.70.10.6347-6351.2004.
25. Tang S, Chan WWM, Fletcher KE, Seifert J, Liang X, Löffler FE, Edwards EA, Adrian L. 2013. Functional characterization of reductive dehalogenases by using blue native polyacrylamide gel electrophoresis. Appl Environ Microbiol 79:974–981. https://doi.org/10.1128/AEM.01873-12.
26. Yang Y, Higgins SA, Yan J, Şimşir B, Chourey K, Iyer R, Hettich RL, Baldwin B, Ogles DM, Löffler FE. 2017. Grape pomace compost harbors organohalide-respiring *Dehalogenimonas* species with novel reductive dehalogenase genes. ISME J 11:2767–2780. https://doi.org/10.1038/ismej.2017.127.
27. Adrian L, Szewzyk U, Wecke J, Görisch H. 2000. Bacterial dehalorespiration with chlorinated benzenes. Nature 408:580–583. https://doi.org/10.1038/35046063.
28. Seshadri R, Adrian L, Fouts DE, Eisen JA, Phillippy AM, Methe BA, Ward NL, Nelson WC, Deboy RT, Khouri HM, Kolonay JF, Dodson RJ, Daugherty SC, Brinkac LM, Sullivan SA, Madupu R, Nelson KE, Kang KH, Impraim M, Tran K, Robinson JM, Forberger HA, Fraser CM, Zinder SH, Heidelberg JF. 2005. Genome sequence of the PCE-dechlorinating bacterium *Dehalococcoides ethenogenes*. Science 307:105–108. https://doi.org/10.1126/science.1102226.
29. Henderson GP, Jensen GJ. 2006. Three-dimensional structure of *Mycoplasma pneumoniae*'s attachment organelle and a model for its role in gliding motility. Mol Microbiol 60:376–385. https://doi.org/10.1111/j.1365-2958.2006.05113.x.
30. Krause DC, Chen S, Shi J, Jensen AJ, Sheppard ES, Jensen GJ. 2018. Electron cryotomography of *Mycoplasma pneumoniae* mutants correlates terminal organelle architectural features and function. Mol Microbiol 108:306–318. https://doi.org/10.1111/mmi.13937.
31. Nakamura S, Aono R, Mizutani S, Takashina T, Grant WD, Horikoshi K. 1992. The cell surface glycoprotein of *Haloarcula japonica* TR-1. Biosci Biotechnol Biochem 56:996–998. https://doi.org/10.1271/bbb.56.996.
32. Bolhuis H, Martín-Cuadrado AB, Rosselli R, Pašić L, Rodriguez-Valera F. 2017. Transcriptome analysis of *Haloquadratum walsbyi*: vanity is but the surface. BMC Genomics 18:510. https://doi.org/10.1186/s12864-017-3892-2.
33. Abdul-Halim MF, Schulze S, DiLucido A, Pfeiffer F, Filho AWB, Pohlschroder M, Albers S-V, Trent MS. 2020. Lipid anchoring of archaeosortase substrates and midcell growth in Haloarchaea. mBio 11:e00349-20. https://doi.org/10.1128/mBio.00349-20.
34. Morris RM, Sowell S, Barofsky D, Zinder S, Richardson R. 2006. Transcription and mass-spectroscopic proteomic studies of electron transport oxidoreductases in *Dehalococcoides ethenogenes*. Environ Microbiol 8:1499–1509. https://doi.org/10.1111/j.1462-2920.2006.01090.x.
35. Krogh A, Larsson B, von Heijne G, Sonnhammer ELL. 2001. Predicting transmembrane protein topology with a hidden Markov model: application to complete genomes. J Mol Biol 305:567–580. https://doi.org/10.1006/jmbi.2000.4315.
36. Pöritz M, Schiffmann Christian L, Hause G, Heinemann U, Seifert J, Jehmlich N, von Bergen M, Nijenhuis I, Lechner U. 2015. *Dehalococcoides mccartyi* strain DCMB5 respires a broad spectrum of chlorinated aromatic compounds. Appl Environ Microbiol 81:587–596. https://doi.org/10.1128/AEM.02597-14.
37. Hartwig S, Dragomirova N, Kublik A, Türkowsky D, von Bergen M, Lechner U, Adrian L, Sawers RG. 2017. A H_2-oxidizing, 1,2,3-trichlorobenzene-reducing multienzyme complex isolated from the obligately organohalide-respiring bacterium *Dehalococcoides mccartyi* strain CBDB1. Environ Microbiol Rep 9:618–625. https://doi.org/10.1111/1758-2229.12560.
38. Yan J, Wang J, Villalobos Solis MI, Jin H, Chourey K, Li X, Yang Y, Yin Y, Hettich RL, Löffler FE. 2021. Respiratory vinyl chloride reductive dechlorination to ethene in TceA-expressing *Dehalococcoides mccartyi*. Environ Sci Technol 55:4831–4841. https://doi.org/10.1021/acs.est.0c07354.
39. Werner JJ, Ptak AC, Rahm BG, Zhang S, Richardson RE. 2009. Absolute quantification of *Dehalococcoides* proteins: enzyme bioindicators of chlorinated ethene dehalorespiration. Environ Microbiol 11:2687–2697. https://doi.org/10.1111/j.1462-2920.2009.01996.x.
40. Kucharzyk KH, Meisel JE, Kara-Murdoch F, Murdoch RW, Higgins SA, Vainberg S, Bartling CM, Mullins L, Hatzinger PB, Löffler FE. 2020. Metagenome-guided proteomic quantification of reductive dehalogenases in the *Dehalococcoides mccartyi*-containing consortium SDC-9. J Proteome Res 19:1812–1823. https://doi.org/10.1021/acs.jproteome.0c00072.
41. Schiffmann CL, Otto W, Hansen R, Nielsen PH, Adrian L, Seifert J, von Bergen M, Jehmlich N. 2016. Proteomic dataset of the organohalide-respiring bacterium *Dehalococcoides mccartyi* strain CBDB1 grown on hexachlorobenzene as electron acceptor. Data Brief 7:253–256. https://doi.org/10.1016/j.dib.2016.02.037.
42. Sung Y, Ritalahti KM, Apkarian RP, Löffler FE. 2006. Quantitative PCR confirms purity of strain GT, a novel trichloroethene-to-ethene-respiring *Dehalococcoides* isolate. Appl Environ Microbiol 72:1980–1987. https://doi.org/10.1128/AEM.72.3.1980-1987.2006.
43. Löffler FE, Ritalahti KM, Zinder SH. 2013. *Dehalococcoides* and reductive dechlorination of chlorinated solvents, p 39–88. *In* Stroo HF, Leeson A, Ward CH (ed), Bioaugmentation for Groundwater Remediation. Springer New York, New York, NY.
44. Clark K, Taggart DM, Baldwin BR, Ritalahti KM, Murdoch RW, Hatt JK, Löffler FE. 2018. Normalized quantitative PCR measurements as predictors for ethene formation at sites impacted with chlorinated ethenes. Environ Sci Technol 52:13410–13420. https://doi.org/10.1021/acs.est.8b04373.
45. Parks DH, Rinke C, Chuvochina M, Chaumeil P-A, Woodcroft BJ, Evans PN, Hugenholtz P, Tyson GW. 2017. Recovery of nearly 8,000 metagenome-assembled genomes substantially expands the tree of life. Nat Microbiol 2:1533–1542. https://doi.org/10.1038/s41564-017-0012-7.
46. Chaumeil PA, Mussig AJ, Hugenholtz P, Parks DH. 2019. GTDB-Tk: a toolkit to classify genomes with the Genome Taxonomy Database. Bioinformatics 36:1925–1927. https://doi.org/10.1093/bioinformatics/btz848.
47. Kalyaanamoorthy S, Minh BQ, Wong TKF, von Haeseler A, Jermiin LS. 2017. ModelFinder: fast model selection for accurate phylogenetic estimates. Nat Methods 14:587–589. https://doi.org/10.1038/nmeth.4285.
48. Minh BQ, Schmidt HA, Chernomor O, Schrempf D, Woodhams MD, von Haeseler A, Lanfear R. 2020. IQ-TREE 2: new models and efficient methods for phylogenetic inference in the genomic era. Mol Biol Evol 37:1530–1534. https://doi.org/10.1093/molbev/msaa015.
49. Quast C, Pruesse E, Yilmaz P, Gerken J, Schweer T, Yarza P, Peplies J, Glockner FO. 2013. The SILVA ribosomal RNA gene database project: improved data processing and web-based tools. Nucleic Acids Res 41:D590–6. https://doi.org/10.1093/nar/gks1219.
50. Edgar RC. 2004. MUSCLE: a multiple sequence alignment method with reduced time and space complexity. BMC Bioinformatics 5:113. https://doi.org/10.1186/1471-2105-5-113.

51. Steenwyk JL, Buida TJ, III, Li Y, Shen X-X, Rokas A. 2020. ClipKIT: A multiple sequence alignment trimming software for accurate phylogenomic inference. PLoS Biol 18:e3001007. https://doi.org/10.1371/journal.pbio.3001007.
52. Letunic I, Bork P. 2019. Interactive Tree Of Life (iTOL) v4: recent updates and new developments. Nucleic Acids Res 47:W256–W259. https://doi.org/10.1093/nar/gkz239.
53. May HD, Miller GS, Kjellerup BV, Sowers KR. 2008. Dehalorespiration with polychlorinated biphenyls by an anaerobic ultramicrobacterium. Appl Environ Microbiol 74:2089–2094. https://doi.org/10.1128/AEM.01450-07.
54. May HD, Sowers KR. 2016. "*Dehalobium chlorocoercia*" DF-1—from discovery to application, p 563–586. *In* Adrian L, Löffler FE (ed), Organohalide-Respiring Bacteria. Springer Berlin Heidelberg, Berlin, Heidelberg.
55. Löffler FE, Sanford RA, Ritalahti KM. 2005. Enrichment, cultivation, and detection of reductively dechlorinating bacteria. Methods Enzymol 397:77–111. https://doi.org/10.1016/S0076-6879(05)97005-5.
56. Chen G, Kleindienst S, Griffiths DR, Mack EE, Seger ES, Löffler FE. 2017. Mutualistic interaction between dichloromethane- and chloromethane-degrading bacteria in an anaerobic mixed culture. Environ Microbiol 19:4784–4796. https://doi.org/10.1111/1462-2920.13945.
57. Chen G, Fisch AR, Gibson CM, Erin Mack E, Seger ES, Campagna SR, Löffler FE. 2020. Mineralization versus fermentation: evidence for two distinct anaerobic bacterial degradation pathways for dichloromethane. ISME J 14:959–970. https://doi.org/10.1038/s41396-019-0579-5.
58. Mastronarde DN. 2005. Automated electron microscope tomography using robust prediction of specimen movements. J Struct Biol 152:36–51. https://doi.org/10.1016/j.jsb.2005.07.007.
59. Kremer JR, Mastronarde DN, McIntosh JR. 1996. Computer visualization of three-dimensional image data using IMOD. J Struct Biol 116:71–76. https://doi.org/10.1006/jsbi.1996.0013.
60. Schindelin J, Arganda-Carreras I, Frise E, Kaynig V, Longair M, Pietzsch T, Preibisch S, Rueden C, Saalfeld S, Schmid B, Tinevez J-Y, White DJ, Hartenstein V, Eliceiri K, Tomancak P, Cardona A. 2012. Fiji: an open-source platform for biological-image analysis. Nat Methods 9:676–682. https://doi.org/10.1038/nmeth.2019.